Arch. Metall. Mater. **71** (2026), 1, 107-116

DOI: https://doi.org/10.24425/amm.2026.157774

D. DEV SINGH[1,4*], SURESH ARJULA[2], A. RAJI REDDY[3], A.K. REVELLY[4]

GRADIENT PATH FUNCTIONALLY GRADED MATERIALS FABRICATED BY DMD USING SS316L AND IN625 POWDERS

Additive Manufacturing (AM) is a layer-by-layer material addition process. Direct Metal Deposition (DMD) is one of the metal powders feeding AM methods. It can produce Functionally Graded Material (FGM) used in extreme service conditions. Two gradient path FGM blocks were deposited by a continuous co-axial nozzle of a commercial DMD machine. Each deposited block was cut into ASTM E8 samples by a wire cut Electric Discharge Machine (EDM). The powders used for deposition were Stainless Steel 316L (SS316L) and Inconel 625 (IN625). The research paper is primarily focused on tensile properties of the samples. The first sample has higher Ultimate Tensile Strength (UTS) of 454 MPa as compared to the second sample and also has higher micro-hardness of 263 HV on its top surface. These properties are due to presence of cellular grains micro-structures in the sample. Fractography revealed that the samples are ductile. However, rounded indications and Face-Centered-Cubic (F.C.C) structure of the specimens have confirmed by radiography test and X-Ray Diffraction (XRD).

Keywords: Functionally Graded Material; Direct Metal Deposition; Stainless Steel 316L; Inconel 625; Ultimate Tensile Strength

1. Introduction

Day-by-day human needs are increasing. To satisfy these needs new technologies have developed. Such as mechanizations, computers, NC machines, lasers, robots, interactive computer graphics, Additive Manufacturing (AM), industry 4.0, and many more [1]. From the last three decades AM is playing a crucial role for manufacturing of customized parts. These parts are printed track-by-track, layer-by-layer and surface-by-surface using selected AM systems [2]. AM has a close interaction with metallurgical and materials science engineering, mechanical engineering, optics and laser engineering, electronics and computer science engineering. Metal AM is basically categorized into powder bed fusion and Direct Energy Deposition (DED). Most of journal papers are covering powder bed fusion followed by DED [3]. Multi-Layer Materials (MLM) of Functionally Graded Material (FGM) produced by DED have cracks and delamination at the interface joints due to variations in co-efficient thermal expansion and thermal residual stresses. To overcome these problems gradient path (i.e., continuous) FGM are introduced [4]. Gradient path Functionally Graded Materials are those materials in which powder compositions can be varied continuously from bottom layer to top to layer. They have varying properties in multiple directions and used in harsh environments. FGM are light weight, high strength, and high temperature gradient, corrosion resistant, novel, heterogeneous, sustainable, and advanced emerging engineering materials. They have superior mechanical and physical performance [5,6]. DED has many advantages due to the variation of powder compositions during the deposition. It is used for production of light weight critical components, FGM, repairing and remanufacturing of sophisticated parts. So, their applications include in aerospace (i.e., gas turbine blades and nozzles), defense (i.e., fabrication of thermal barriers), nuclear reactors (i.e., production of nuclear fuel store components), marine (i.e., fabrication of ship hulls), automotives (i.e., for production of valve stems, pistons, cylinder liners, drive shafts, flywheels, and shock absorbers), machine equipment's (repairing of moulds, dies, cutting tools, and vessels) [7-12]. The use of steels in automotive industry was reduced from 70% to 60% during period of 1996-2000. DED deposition process is ten times faster than the powder bed fusion processes, but the parts have poor dimensional accuracy. This problem can be solved by the use of adaptive control (AC) technology. Hybrid DED also used to produce multi-layer materials of electronics parts [13-16]. However, the applications

[1] JAWAHARLAL NEHRU TECHNOLOGICAL UNIVERSITY, DEPARTMENT OF MECHANICAL ENGINEERING, HYDERABAD 500085, INDIA
[2] JNTUH UNIVERSITY COLLEGE OF ENGINEERING, DEPARTMENT OF MECHANICAL ENGINEERING, JAGITIAL 505501, INDIA
[3] DEPARTMENT OF MECHANICAL ENGINEERING, CMR TECHNICAL CAMPUS, HYDERABAD 501401, INDIA
[4] RAJIV GANDHI UNIVERSITY OF KNOWLEDGE TECHNOLOGIES, DEPARTMENT OF METALLURGICAL AND MATERIALS ENGINEERING, BASAR 504107, INDIA

* Corresponding author: devsingh209@gmail.com

of this technology are limited till now also, because of lack of knowledge to understand the process mechanism. The process mechanism (i.e., powder flow rate, melt-pool generation and solidification) involved with many inter related parameters [17]. For considering selling of all types of DED systems, it is only 8% as compared to 82% of powder bed fusion systems [18]. The classifications of FGM are i. Thin and thick FGM, ii. Structurally graded and compositionally graded FGM, iii. Compositionally graded FGM are Multi-Layer Materials (MLM) and gradient path FGM, iv. Based on dimensions, they are 1D, 2D and 3D FGM, v. Fraction, shape, orientation and size gradient type FGM.

It is possible to generate a consistent melt-pool by varying laser power and powder feed rate using a powder fed DED process. But, the deposited parts are subjected to cyclic heating and cooling during the process and form complex micro-structures. These micro-structures are unable to analyze to predict the mechanical properties as compared to conventional ones. So, there is need to develop artificial intelligence and machine learning algorithms for DED process from pre-processing to post-processing [19,20]. There is lack of AM standards in DED and none of the CAD packages are available for the creation of heterogeneous models. Adaptive slicing methods for powder bed fusion, multi-direction slicing and non-layer wise slicing methods for DED are not well developed till now [21,22].

Today's globalization industries prefer the use of Industry 4.0. Industry 4.0 allows decentralized AM processes for saving time and cost. It integrates AM systems with industrial internet of things, cloud computing, and Big Data analysis. So, it can focus on advancement in material science and design, development of manufacturing processes, supply chain management, and business models [23-25]. Now the attention is required on AM in terms of socio-economic and environmental sustainability. For easy assessment of AM, a software model of Sustainable Value Roadmapping Tool (SVRT) was also developed [26,27].

A gradient path FGM was deposited by a DED machine with gradual variation of compositions form low carbon steel at the bottom to austenitic Stainless Steel 316L (SS316L) at the top. There were no cracks and delamination observed among the deposited layers. The micro-tensile test report revealed that the sample had an excellent strength and ductility combination of Ultimate Tensile Strength (UTS) of 880 MPa and an elongation of 80% respectively [28]. One of the simple strategies to improve the tensile properties of DED processed austenitic SS316L is the addition of Ti to the required quantity. The sample deposited with 2 wt.% of Ti had yield strength (YS), UTS and elongation of 637 MPa, 857 MPa and 43% respectively [29]. Another FGM block with ferrite P21 and austenite SS316L was deposited using DED by varying composition continuously from bottom to top. Micro-tensile report of the FGM showed slightly higher UTS of 619 MPa as compared to the value 616 MPa of pure SS316L [30-32]. A discrete FGM was also fabricated by a DED process using ferrite SS430 and austenite SS316 steel powders. The magnetic response, porosity, and residual stress variation were evaluated [33]. The UTS of 1029 MPa, YS of 822 MPa, and micro-hardness range 216 HV to 355 HV for gradient path FGM with continuous variation of SS316L to Inconel 625 (IN625) powders was produced by using laser direct metal deposition [34]. During the production of continuous FGM using SS316L and IN625 powders by a DED process, it is better to start depositing first with SS316L on the substrate and then vary their compositions to the required quantity toward top of the sample. If doing so, high density IN625 particles can mix easily into the low density SS316L particles in the melt-pool. This can form equiaxed grains and lead better mechanical properties [35]. A five layered thin wall FGM was deposited by direct laser metal deposition machine with continuous variation of SS316L and IN625 powders. The highest width (i.e., 1.6 mm) and height (i.e., 6.4 mm) of the layers was obtained at the highest laser power of 280 W. The micro-hardness of gradient wall was changing from 225 HV to 277 HV [36].

Transition joint sample as well as composition gradually varying sample with SS316 and IN625 powders, individual pure SS316 and pure IN625 samples were deposited by laser engineered net shaping. The samples produced based on discrete and continuous deposition and their tensile properties are compared with lower strength materials. The YS and UTS of a discrete specimen (i.e., 298 MPa, 539 MPa) and a continuously graded specimen (i.e., 306 MPa, 537 MPa) are comparable to the strength of pure SS316 sample (i.e., 285 MPa, 557 MPa) and pure IN625 sample (514 MPa, 934 MPa) [37]. The transition joint samples were deposited by a DED process using SUS316L and IN625 powders and obtained UTS of 550 MPa and micro-hardness variation 200 HV to 430 HV [38]. The dissimilar materials of SS316L and IN625 were joined by the introduction of a single compositional layer in the middle of the specimen using a powder composition of 50% SS316L and 50% IN625 by a DED machine. It was found that UTS, YS, and variation in micro-hardness were 605 MPa, 405 MPa, and 170 HV to 210 HV respectively [39]. A bionic mechanical interlocking multi-layer material FGM using SS316L and IN625 powders was deposited by a DED process. Here, soft layers absorb energy and hard layers dissipate it during the loading and reduce the crack propagation. The UTS of the FGM was 675 MPa as compared to its pure SS316L (647 MPa) [40]. Structural gradient multi-metal FGM was produced by laser powder bed fusion using IN625 and SS316L powders. The micro-hardness was gradually varying from SS316L region (237 HV) to IN625 region (285 HV) [41]. Another name of FGM is Functionally Integrated Materials (FIM). A transition joint was formed by depositing pure SS316L and pure Hynes 282 at the bottom and top respectively using a DED method. But, it has sharp interface edges. This was eliminated by depositing multi-layer materials with 10% SS316L + 90% Hynes 282 and 50% SS316L + 50% Hynes 282 in the respective samples [42].

A FGM was deposited by a DED machine with continuous variation of SS316L and IN718 without any cracks. Its hardness was varied from 250 HV to 290 HV [43]. The similar FGM was deposited by laser engineered net shaping using in-situ powder mixing in the melt-pool. When it is deposited with 23% SS316L + 77% IN718, fine grain micro-structures were observed in the

sample. This is one of the ways to develop new alloys. Neural networks based ThermoCalc® software is also used for calculating alloy compositions [44-46]. A DED system deposited single composition SS316L samples. It was observed that powder deposition increases with increasing laser power and it promotes porosity. It can control by reversing these parameters. Due to repetitive heating and cooling of the samples, grain growth was increased three times. The mechanical properties such as UTS, YS, and hardness of the samples produced in horizontal build direction with high scan speed and low laser power are varying in the range of 545-634 MPa, 448-455 MPa, and 220-260 HV [47,48]. One of the structural and cladding materials used for nuclear reactor components was grade 91 steel powders. It was deposited in cubed shape of 15 mm × 15 mm × 15 mm by a DED process. The micro-hardness of the sample showed an average hardness of 349 HV. Its micro-tensile sample exhibited high UTS of 900 MPa as compared to its wrought grade 91 part (730 MPa) [49]. High entropy alloys manufactured by DED and powder bed fusion consist of un-melted powder particles, micro-pores, residual stresses, and coarse micro-structures. These can be reduced by post processing methods like hot isostatic pressing, annealing, aging, and deep cryogenic treatments. This work was proposed the use of light weight refractory for coating, which is known as compositionally graded high entropy alloys [50]. Not only high entropy alloys, ceramics also deposited as coating by a DED process even though there are brittle and having high melting point [51]. The maximum volume of a component produced by powder bed fusion and DED was 400 mm^3 and 3200 mm^3 respectively. There are three types of deposition nozzles in DED machines equipped with pneumatic (i.e., Argon or Neon gas) powder feeders. They are lateral, discrete coaxial and continuous coaxial nozzles. The last one is most widely used in many DED systems because of it high powder captures efficiency and independent of deposited tracks from the direction of deposition [52-54].

The present paper is organized as follows. The basic concepts, properties of FGM deposited with various combinations of metal powders such as low carbon steel, SS316, SS316L, SS430, IN625, Inconel 718 (IN718), ferrite P21, and Hyness 282 by various authors are discussed in the section 1. Section 2 illustrated the combination of SS316L and IN625 metal powders used for the deposition of gradient path FGM blocks and the characterization of the ASTM E8 samples. However, section 3 explained macro-structure, micro-structure, micro-tensile test, micro-hardness, factography, radiography and XRD of the samples. XRD can reveal lattice structure any material [55]. At last, the section 4 indicated the conclusions. The terms transition joint, discrete, and discontinuous variation refers to multi-layer materials FGM. However, the terms gradual variation, varying composition, and continuous variation refers to gradient path FGM and also the words sample and specimen are interchangeably used in this paper.

The present research is focused on gradient path FGM made of SS316L and IN625 powders, a material utilized in extreme service conditions such as resistance to corrosion and existence of high temperature gradient. The rationale is perfect joining of two dissimilar materials of SS316L and IN625 by DMD than a conventional welding process. The present work aim is to reveal micro-structural and mechanical properties of continuously graded FGM manufactured by DMD. The FGM samples are produced based on thick layer (i.e., thickness more than 1 mm) of deposition. It is concluded that sample-1 has higher UTS and sample-2 possessed maximum YS, breaking strength (BS) and percentage of elongation. The elemental composition detected by an Octane Elite Energy Dispersive X-ray Analysis (EDAX) coincides with powder composition used during the deposition. This paper is also analysed fractography, radiography and XRD of the ASTM E8 FGM samples.

2. Experimentation

2.1. Materials and methods

The metal powders of SS316L and IN625 were used by DMD for gradient path deposition of FGM blocks. Gradient path Functionally Graded Materials are those materials in which powder compositions can be varied continuously from bottom layer to top to layer. Fig. 1(a) and Fig. 1(b) have shown that both the powders have gas atomized spherical shape particles of size in the range of 50-150 microns. The primary advantage of

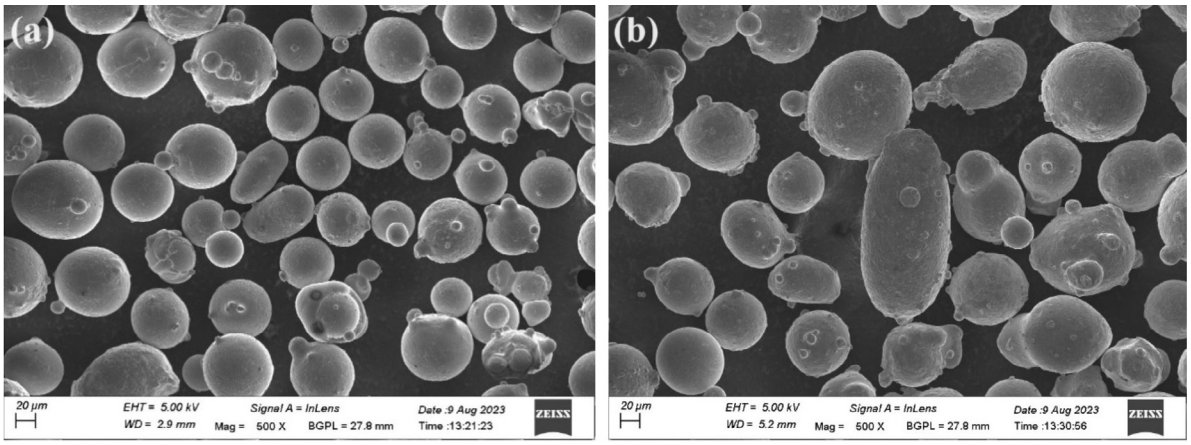

Fig. 1. Powder morphology of selected (a) stainless steel and (b) inconel powders

using SS316L and IN625 powders is high corrosion resistance and high temperature resistance respectively. The first layer deposited on the stainless steel substrate was pure SS316L powder. In the middle, thirteen layers were deposited with thirteen alloy compositions of SS316L and IN625 powders. Finally, on top of the blocks pure IN625 powder was deposited. The significance of FGM used in additive manufacturing in the context DMD is, they have multi-directional properties when they exposed to different environment conditions. The metal powders were preheating up to 60°C for 10 minutes before filled into the powder hopper. The deposition machine utilized for SS316L and IN625 metal powders was DMD machine. It has a continuous co-axial nozzle of 485 mm focal length with 23 mm standup distance. The laser line (LDF4.000-30) production unit produced diode laser for 5 mm beam spot using the power capacities range 100 W to 4000 W. The deposition head with a scan speed of 10-30 mm/s and powder feed rate of 15-50 g/min was used for thick layer of deposition. The deposited layers hatch spacing was 2 mm. Chilled distilled water at 15°C supplied with 10 liters per minutes was used for cooling the deposition head. Argon gas was used as carrier and shielding gas for moving powders from the hopper to nozzle, protecting laser beam and melt-pool.

2.2. Gradient path functionally graded materials

In gradient path FGM blocks, the deposited powder compositions were varied continuously from bottom to top in each layer. Based on the selected two parameter sets showed in TABLE 1, two gradient path FGM blocks of size 26 mm × 34 mm × 32 mm (width × thick × height) were deposited based on thick layer of deposition by a commercial DMD machine. There were fifteen layers in each FGM block printed vertically with bi-directional scanning. The bottom layer and top layer were printed with pure SS316L and pure IN625 powders respectively. The remaining thirteen layers with different powder compositions were printed in the middle of the blocks. Fig. 2 has shown one of the gradient path FGM blocks deposited by the DMD machine. For more details about these layers refer the section 3.1. The selected two parameter sets were at medium and high laser power available on the DMD machine. It has indicated that for thick layer of deposition, low constant scan velocity was selected to melt the powder particles in steady state melt pool at these laser powers. By maintaining constant deposition speed, the laser beam has sufficient time and heat energy to melt all metal powder particles completely at the deposition region. Hence, it can promote strong metallurgical bonds among metal powder particles and leads to better mechanical properties. The laser beam, which is melting powder particles, can also obey the Gaussian distribution of heat energy. The constant speed selected for deposition of FGM block-1 and FGM block-2 is 10 mm/s. It is the lowest speed on the de DMD machine for generating steady state melt pool. The current limitations of using DMD for fabricating FGMs are that it cannot produce smooth surface parts and large components. So, research is going on to produce smooth surface parts and large components in future.

Fig. 2. Deposition of gradient path FGM block based on first experimental parameter set

TABLE 1

Selection of parameter sets for printing

Expt. No.	Parameters		
	Laser power (P), W	Scan velocity (V), mm/s	Powder feed rate (M), g/min
1	2500	10	25
2	3500	10	30

2.3. Characterization

The gradient path ASTM E8 FGM samples were tensile tested perpendicular to the deposition direction by a 250 KN capacity SHIMADZU micro-tensile machine. The load applied on these specimens was at the rate of 5 mm/min based on the ASTM E8 standards. Fig. 3(a) and Fig. 3(b) have shown ASTM E8 tensile specimens of size having 9 mm wide, 3 mm thickness, and 30 mm height with a gauge length of 10 mm were cut by an Electronica CNC wire cut EDM from the two FGM blocks respectively.

Micro-hardness of these two gradient path specimens was determined by VH-1DMX model, ECONOMET hardness tester. The load applied capacity of the equipment by a diamond pyramid indenter was ranging from 5 g to 1 kg. In this test, the indenter applied a load of 500 g for 15 s at the center of 30 mm height specimen perpendicular to the deposition direction for 0.5 mm intervals. The Fig. 4 has shown the deposited layers in a better way from the macro-structural image of the sample-1 captured by an Olympus optical microscopy. The distribution of phases in various layers of the samples is known by the micro-structural examinations. The factography of samples at different magnifications were taken by GeminiSEM500 instrument. The elemental analysis was carried out by an Octane Elite EDAX with help of GeminiSEM500 instrument. The radiography and XRD analyses were also performed on these ASTM E8 FGM samples.

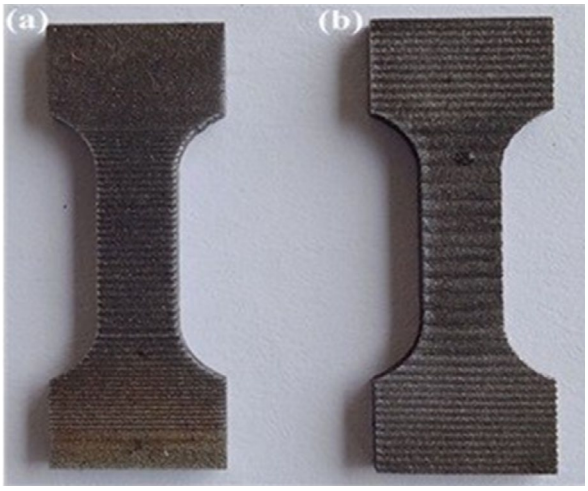

Fig. 3. ASTM E8 FGM (a) sample-1 and (b) sample-2 obtained from respective FGM blocks

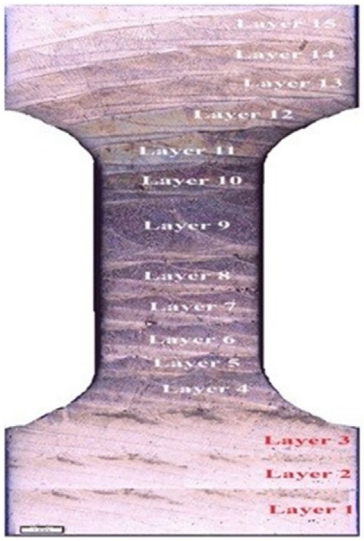

Fig. 4. Macro-structure of ASTM E8 FGM sample-1

3. Results and discussions

3.1. Macro-structure

There were fifteen layers in each gradient path FGM sample. The layer-1 and layer-15 were deposited with pure SS316L and pure IN625 powders respectively. For remaining thirteen layers, the alloy compositions prepared using SS316L and IN625 powders are listed TABLE 2. Fig. 4 has shown macro-structure of fifteen layers of the sample-1 taken by an Olympus optical microscopy. Its deposited layers thickness and hatch spacing were 1.3 mm and 2 mm respectively. These two values are also same for the second sample.

TABLE 2

Powder compositions by percentage of weight

Layer's	Percentage of alloy compositions
1	100% SS316L
2	92.86% SS316L + 7.14% IN625
3	85.72% SS316L + 14.28% IN625
4	78.58% SS316L + 21.42% IN625
5	71.44% SS316L + 28.56% IN625
6	64.30% SS316L + 35.70% IN625
7	57.16% SS316L + 42.84% IN625
8	50.02% SS316L + 49.98% IN625
9	42.88% SS316L + 57.12% IN625
10	35.74% SS316L + 64.26% IN625
11	28.60% SS316L + 71.40% IN625
12	21.46% SS316L + 78.54% IN625
13	14.32% SS316L + 85.68% IN625
14	7.18% SS316L + 92.82% IN625
15	100% IN625

3.2. Micro-structure

The micro-structures of gradient path FGM samples on selected seven different compositional layers were taken by an Olympus optical microscopy. Fig. 5 has shown the micro-structures of ninth layer of the sample-1. Fig. 5(a) depicted the cellular grains micro-structure, and Fig. 5(b) has shown the fine grains micro-structure. But second sample-2 has shown coarse cellular grains micro-structure. The presence of cellular grains microstructure in the sample can promotes better material properties than the samples having columnar grains microstructure. The white regions are representing austenite phases and dark areas compressing compounds of SS316L and IN625 in the micro-structures.

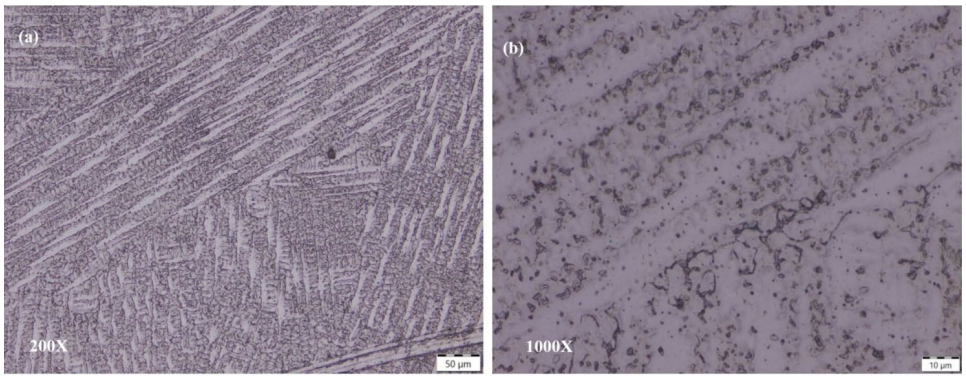

Fig. 5. Micro-structures of sample-1 viewed at (a) 200× and (b) 1000×

3.3. Micro-tensile test

Micro-tensile tests were performed on ASTM E8 samples taken from each FGM block. Fig. 6(a) and Fig. 6(b) have shown the fractured samples of the respective FGM blocks. The measured values of mechanical properties such as UTS, YS, BS, percentage of reduction in area and strain were listed in TABLE 3. From the micro-tensile report, it was analyzed that the sample-1 had higher UTS of 454 MPa as compared to sample-2. But the sample-2 had maximum YS (205 MPa), BS (343 MPa), percentage of reduction in area (13%) and percentage of strain (29%). Based on the maximum percentage of reduction in area and strain, it has decided that the sample-2 was more ductile. The reasons for exhibiting higher ductility of the second sample are, it may be due to strain gradient induced by heterogeneous deformation activates additional slip systems and the carbon powder particles present in that sample may be acts as lubricant to deform more. The thick layered gradient path FGM sample-1 and sample-2 were fractured in the compositional zone of 50% SS316L + 50% IN625 (i.e., eighth layer) at a distance of 14.46 mm and 15.52 mm respectively from their bottom. The cause of the failure of these samples was may be due to high powder feeding rate. The gradual variation in UTS of FGM specimens has indicated good metallurgical bonding among the layers of the samples.

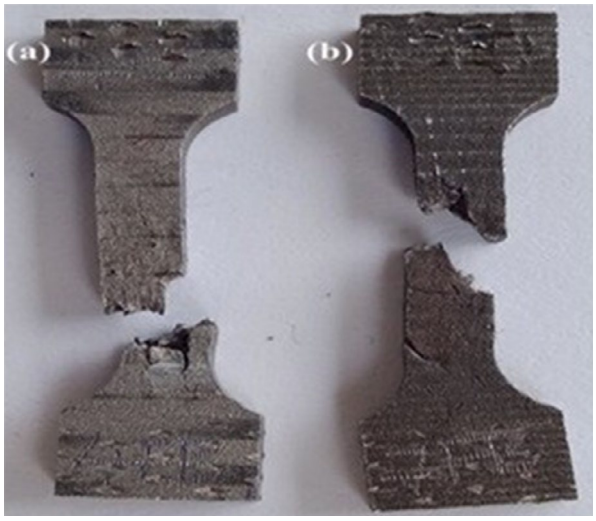

Fig. 6. Failure of ASTM E8 (a) sample-1 and (b) sample-2 of respective FGM blocks

TABLE 3

Mechanical properties of tensile failure samples

Samples of the Expt. No.	UTS (MPa)	YS (MPa)	BS (MPa)	% of reduction in area	% of strain
1	454	167	306	12	28
2	402	205	343	13	29

3.4. Micro-hardness

Fig. 7 depicted the gradual variation in micro-hardness of each sample of the respective FGM blocks. It is gradually increasing as the content of IN625 increases. Fig. 7(a) has shown change in micro-hardness from 172 HV (minimum) to 263 HV of the sample-1. The maximum hardness of 263 HV was evaluated on the top layer of this sample. It may be due to formation of fine grains micro-structure in it and lead to better micro-hardness. This micro-hardness value was more than the micro-hardness of the sample (164 HV-255 HV) produced in the research work of W. Meng et al. [56] and also within the range of 216 HV to 355 HV in the research work carried out by B. Chen et al [34]. Another main reason for continuously varied/increased micro-hardness in the FGM sample-1 was sufficient laser power to melt the powder particles for forming strong metallurgical bonds. Hence, it has also higher UTS as compared to sample-2. The micro-hardness of the sample-2 as shown in Fig. 7(b) printed at high powder feed rate with high laser power was varying from 168 HV (minimum) to a maximum of 236 HV.

3.5. Fractography

The surface morphology of gradient path FGM sample-1 fractured in the eighth compositional layer had observed by a scanning electron microscopy of GeminiSEM500. Fig. 8 had shown its surface morphology at two different magnifications. Fig. 8(a) had depicted with void, micro-holes and micro-cracks. However, Fig. 8(b) had shown the formation of debris, many numbers of simple and smeared shallows. The uniform surface morphology with simple and smeared shallows was indicated

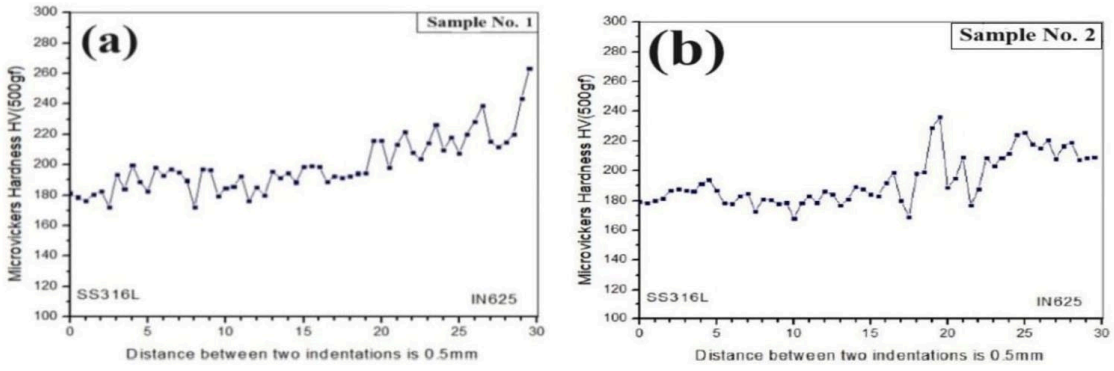

Fig. 7. Micro-hardness variation of gradient path ASTM E8 (a) sample-1 and (b) sample-2

truly the ductile fracture with poor deformation of the first sample and also of the second sample.

The broken surface of the two specimens from the respective FGM blocks was selected for micro-structural and elemental analysis by GeminiSEM500 instrument and Octane Elite EDAX respectively. For element analysis of the samples, two spots were selected on the fractured surfaces. It was observed that 2.34% of Molybdenum content present in the selected locations. The presence of this quantity of Molybdenum was also within the range of 2-9% in these samples when compared with SEM powder morphology report and datasheet of powder supplier. The elemental compositions at those locations were also matched with its manually prepared powder composition. It has indicated that good metallurgical bonding exist between the layers of the samples. Fig. 9(a) and Fig. 9(b) have shown the microstructure taken by the SEM and elemental distribution evaluated by EDAX at the fractured surface of the sample-1 respectively. The EDAX report revealed that the two samples had maximum amount of iron (Fe), followed by chromium (Cr), and nickel (Ni).

3.6. Radiography

Radiography is a Non Destructive Testing (NDT) method uses either X-rays or gamma rays. It is classified into two types. They are Digital Radiography (DR) and Computer Tomography (CT). Digital Radiography is used to identify any flaws or defects in a specimen. However, Computer Tomography is costlier and a most powerful tool for geometry validation. In this present characterization, gradient path ASTM E8 samples made of SS316L and IN625 powders were kept under the radiographic equipment between the X-ray radiation source and the film of size 76.2 mm × 101.6 mm (or detector). Based on the ASTM E446 testing procedure, it was observed that first sample has one rounded indication and second sample consists of six rounded indications. The rounded indications represent defects such as porosities and blowholes. Hence, it is conformed that sample-1 has higher UTS than sample-2.

3.7. X-Ray Diffraction

The XRD is a powerful method for characterization of materials. It can be utilized to find crystal structures and lattice parameters. The Modern XRD systems run completely by a diffractometer and store the diffraction data of a material in its memory. The output can suggest the possible phases and types of materials. Generally, austenitic SS316L and IN625 powder materials are having face-centered-cubic (F.C.C) structures with lattice parameter of 3.5960 Å and 3.6009 Å respectively. In the present work, XRD characterization was done by BRUKER D8 DISCOVER XRD machine on gradient path FGM samples made of SS316L and IN625 powders and found lattice parameter of 3.599 Å and 3.596 Å respectively. For more details about the specimen, refer its macro-structure as shown in TABLE 2. The XRD peak profiles with crystal planes of FGM sample-1 and sample-2 are given Fig. 10(a) and Fig. 10(b). It is also included as shown in TABLE 4 and TABLE 5 about 2θ, d-spacing, Full Width at Half Maximum (FWHM), crystallite size, miller planes for sample-1 and sample-2 with reference to the ICDD card numbers of SS316L and IN625 are PDF-00-033-0397 and PDF-01-071-8710 respectively.

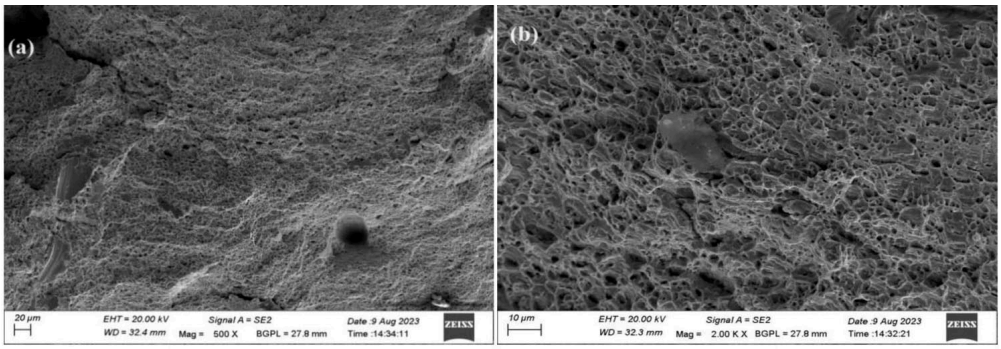

Fig. 8. Fractograph of sample-1 viewed at (a) 500× and (b) 2000× using SEM

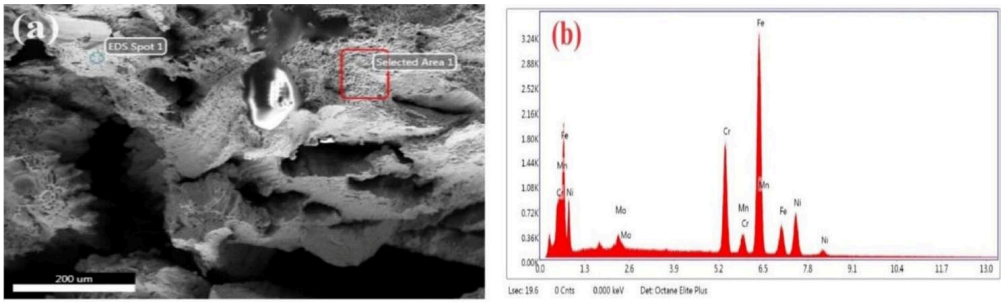

Fig. 9. The failure SEM image of (a) specimen-1 and (b) its elemental distribution displayed by EDAX

TABLE 4

The XRD parameters for gradient path FGM sample-1 and sample-2 (laser power 2500 W)

Phase	Plane (hkl)	2θ (°)	FWHM values (°)	d-spacing values (Å)	Crystalline size, D (nm)
SS316L	(111)	43.5	0.1	2.087	89.30
SS316L	(200)	50.5	0.25	1.808	36.68
SS316L	(220)	74.5	0.25	1.278	41.69

TABLE 5

The XRD parameters for gradient path FGM sample-1 and sample-2 (laser power 3500 W)

Phase	Plane (hkl)	2θ (°)	FWHM values (°)	d-spacing values (Å)	Crystalline size, D (nm)
IN625	(111)	43.5	0.1	2.087	89.30
IN625	(200)	50	0.3	1.808	30.51
IN625	(220)	75	0.15	1.278	69.71

4. Conclusions

Two gradient path FGM blocks with fifteen different compositional layers are deposited successfully using a commercial DMD machine. Based on the mechanical properties and characterization of the FGM ASTM E8 samples, these conclusions are drawn. The micro-tensile reports revealed that sample-1 has higher UTS of 454 MPa as compared to sample-2. However, the sample-2 has maximum yield strength of 205 MPa, breaking strength of 343 MPa and ductility. The micro-hardness of these samples is increased from their bottom to top surfaces as the content of IN625 increased. It has observed higher microhardness value of 263 HV at the top surface for the first sample. Hence, these samples are sustainable for harsh environments.

An Olympus optical microscope has shown cellular grain micro-structures on these samples at the selected magnifications. The GeminiSEM500 image of the fractured samples has shown that the uniform size shallows representing ductile failure. The Octane Elite EDAX report revealed that the Molybdenum content (i.e., 2.34%) at the fractured surface was within the range of 2-9 % as compared to powder supplier reports. Based on the ASTM E446 radiographic standard testing procedure, it was revealed that first sample has one rounded indication and second sample consists of six rounded indications. So, these are the conformations that sample-1 has higher UTS than sample-2. These FGM samples made of SS316L and IN625 powders have shown the face-centered-cubic (F.C.C) crystal structure in the diffraction output information.

Acknowledgement

One of the Authors (D. Dev Singh) would like to express thanks to RGUKT (IIIT Basar) and management of CMR Technical Campus, Hyderabad for their support during this work.

REFERENCES

[1] D. Singh, T. Mahender, A. Raji Reddy, Mater. Today Proc., Powder bed fusion process: a brief review. Materials Today: Proceedings **46** (1), 350-355 (2021). DOI: https://doi.org/10.1016/j.matpr.2020.08.415

[2] D.G. Ahn, Directed energy deposition (DED) process: state of the art. Int. J. Precis. Eng. Manuf.-Green Tech. **8** (2), 703-742 (2021). DOI: https://doi.org/10.1007/s40684-020-00302-7

[3] Zhai. X, Jin. L, Jiang. J, A survey of additive manufacturing reviews. Mater. Sci. Addit. Manuf. **1** (4), 1-22 (2022). DOI: https://doi.org/10.18063/msam.v1i4.21

[4] S.W. Yang, J. Yoon, H. Lee, D.S. Shim, Defect of functionally graded material of Inconel 718 and STS 316L fabricated by directed energy deposition and its effect on mechanical properties. J. Mater. Res. Technol. **17**, 478-497 (2022). DOI: https://doi.org/10.1016/j.jmrt.2022.01.029

[5] Y. Zhu, K. Ameyama, P.M. Anderson, I.J. Beyerlein, H. Gao, H.S. Kim, Heterostructured materials: superior properties from hetero-zone interaction. Mater. Res. Lett. **9** (1), 1-31 (2021). DOI: https://doi.org/10.1080/21663831.2020.1796836

[6] K. Kumar, S. Dixit, Md. Zia ul Haq, A. Stefanska, S.K. Tummala, P.B. Bobba, N. Kaur, M.A. Mohiuddin, From homogeneity to heterogeneity: designing functionally graded materials for advanced engineering applications. E3S Web Conf. **430**, 01198 (2023). DOI: https://doi.org/10.1051/e3sconf/202343001198

[7] J. Bi, L. Wu, S. Li, Z. Yang, X. Jia, M.D. Starostenkov, G. Dong, Beam shaping technology and its application in metal laser additive

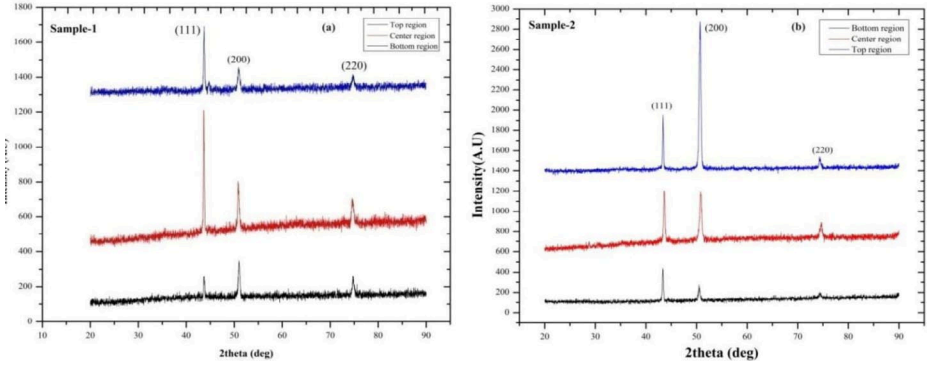

Fig. 10. XRD analysis results of FGM (a) sample-1 and (b) sample-2

manufacturing: a review. J. Mater. Res. Technol. 26, 4606-4628 (2023). DOI: https://doi.org/10.1016/j.jmrt.2023.08.037

[8] Z. Kolozsváry, The relationship between materials science and the fourth industrial revolution. Acta Mater. Transylv. **2** (1), 1-68 (2019). DOI: https://doi.org/10.33924/amt-2019-01-01

[9] G. Tosic, G. Bogdanovic, D. Cukanovic, A. Radakovic, Functionally graded materials in transport vehicles – overview, fabrication, application, modeling. IOP Conf. Ser.: Mater. Sci. Eng. 1271 (2022).

[10] B. Saleh, J. Jiang, R. Fathi, T. Al-Hababi, Q. Xu, L. Wang et al., 30 years of functionally graded materials: an overview of manufacturing methods, applications and future challenges. Compos. B Eng. **201**, 1-46 (2020).
DOI: https://doi.org/10.1016/j.compositesb.2020.108376

[11] A. Saboori, A. Aversa, G. Marchese, S. Biamino, M. Lombardi, P. Fino, Application of directed energy deposition-based additive manufacturing in repair. Appl. Sci. **9** (16), 1-26 (2019).
DOI: https://doi.org/10.3390/app9163316

[12] C. Guo, L. Gan, S. Li, X. Hu, H. Lu, X. Li, Additive manufacturing of Ni-based superalloys: residual stress, mechanisms of crack formation and strategies for crack inhibition. Nano Mater. Sci. **5** (1), 53-77 (2023).
DOI: https://doi.org/10.1016/j.nanoms.2022.08.001

[13] T.C. Dzogbewu, N. Amoah, J.S. Afrifa, S.K. Fianko, J. de Beer, Multi-material additive manufacturing of electronic components: a bibliometric analysis. Results Eng. **19**, 1-18 (2023).
DOI: https://doi.org/10.1016/j.rineng.2023.101318

[14] R. Shanthar, K. Chen, C. Abeykoon, Powder-based additive manufacturing: a critical review of materials, methods, opportunities and challenges. Adv. Eng. Mater. **25** (19), 1-43 (2023).
DOI: https://doi.org/10.1002/adem.202300375

[15] V. Monfared, S. Ramakrishna, N. Nasajpour-Esfahani, D. Toghraie, M. Hekmatifar, S. Rahmati, Science and technology of additive manufacturing progress: processes, materials and applications. Met. Mater. Int. **29**, 1-29 (2023).
DOI: https://doi.org/10.1007/s12540-023-01467-x

[16] H. Wang, W. Liu, Z. Tang, Y. Wang, X. Mei, K.M. Saleheen et al., Review on adaptive control of laser-directed energy deposition. Opt. Eng. **59** (7), 1-18 (2020).
DOI: https://doi.org/10.1117/1.OE.59.7.070901

[17] G. Piscopo, E. Atzeni, A. Saboori, A. Salmi, An overview of the process mechanisms in the laser powder directed energy deposition. Appl. Sci. **13** (1), 1-37 (2023).
DOI: https://doi.org/10.3390/app13010117

[18] G. Piscopo, L. Iuliano, Current research and industrial application of laser powder directed energy deposition. Int. J. Adv. Manuf. Technol. **119** (11-12), 6893-6917 (2022).
DOI: https://doi.org/10.1007/s00170-021-08596-w

[19] S.S. Babu, A.H.I. Mourad, K.H. Harib, S. Vijayavenkataraman, Recent developments in the application of machine-learning towards accelerated predictive multiscale design and additive manufacturing. Virtual Phys. Prototyp. **18** (1), 1-47 (2023).
DOI: https://doi.org/10.1080/17452759.2022.2141653

[20] K. Wasmer, M. Wüst, D. Cui, G. Masinelli, V. Pandiyan, S. Shevchik, Monitoring of functionally graded material during laser directed energy deposition by acoustic emission and optical emission spectroscopy using artificial intelligence. Virtual Phys. Prototyp. **18** (1), 1-21 (2023).
DOI: https://doi.org/10.1080/17452759.2023.2189599

[21] D.E.P. Klenam, O.S. Bamisaye, I.E. Williams, J.W. Van der Merwe, M.O. Bodunrin, Global perspective and African outlook on additive manufacturing research – an overview. Manuf. Rev. **9** (35), 1-37 (2022).
DOI: https://doi.org/10.1051/mfreview/2022033

[22] J. Xu, X. Gu, D. Ding, Z. Pan, K. Chen, A review of slicing methods for directed energy deposition based additive manufacturing. Rapid Prototyp. J. **24** (6), 1-15 (2018).
DOI: https://doi.org/10.1108/RPJ-10-2017-0196

[23] U.M. Dilberoglu, B. Gharehpapagh, U. Yaman, M. Dolen, The role of additive manufacturing in the era of industry 4.0. Procedia Manuf. **11**, 545-554 (2017).
DOI: https://doi.org/10.1016/j.promfg.2017.07.148

[24] S. Ford, M. Despeisse, Additive manufacturing and sustainability: an exploratory study of the advantages and challenges. J. Clean. Prod. **137**, 1573-1587 (2016).
DOI: https://doi.org/10.1016/j.jclepro.2016.04.150

[25] W.E. Frazier, Metal additive manufacturing: a review. J. Mater. Eng. Perform. **23** (6), 1917-1928 (2014).
DOI: https://doi.org/10.1007/s11665-014-0958-z

[26] M. Despeisse, M. Yang, S. Evans, S. Ford, T. Minshall, Sustainable value roadmapping framework for additive manufacturing. Procedia CIRP **61**, 594-599 (2017).
DOI: https://doi.org/10.1016/j.procir.2016.11.186

[27] D.J. Horst, A.D. Charles, R. Almeida Vieira, Additive manufacturing at industry 4.0: a review. Int. J. Eng. Techn. Res. **8** (8), 3-8 (2018).

[28] G. Shin, M. Ebrahimian, N.K. Adomako, H. Choi, D.J. Lee, Y. Ji-Hyun et al., Microstructural evolution and mechanical properties of functionally graded austenitic-low-carbon steel produced via directed energy deposition. Mater. Des. **227**, 111681 (2023).
DOI: https://doi.org/10.1016/j.matdes.2023.111681

[29] S.B. Han, Y.S. Lee, S.H. Park, H. Song, Ti-containing 316L stainless steels with excellent tensile properties fabricated by directed energy deposition additive manufacturing. Mater. Sci. Eng. A **862**, 144414 (2023).
DOI: https://doi.org/10.1016/j.msea.2022.144414

[30] M. Jo, H.S. Kim, J.Y. Park, S.G. Lee, B.J. Kim, H.C. Kim et al., Microstructure and mechanical properties of P21-STS316L functionally graded material manufactured by direct energy deposition 3D print. Metals **12** (12), 1-17 (2022).
DOI: https://doi.org/10.3390/met12122086

[31] D.K. Kim, W. Woo, E.Y. Kim, S.H. Choi, Microstructure and mechanical characteristics of multi-layered materials composed of 316L stainless steel and ferritic steel produced by direct energy deposition. J. Alloys Compd. **774**, 896-907 (2019).
DOI: https://doi.org/10.1016/j.jallcom.2018.09.390

[32] W. Woo, D.K. Kim, E.J. Kingston, V. Luzin, F. Salvemini, M.R. Hill, Effect of interlayers and scanning strategies on through-thickness residual stress distributions in additive manufactured ferritic-austenitic steel structure. Mater. Sci. Eng. A **744**, 618-629 (2019). DOI: https://doi.org/10.1016/j.msea.2018.12.078

[33] B. Heer, A. Bandyopadhyay, Compositionally graded magnetic-nonmagnetic bimetallic structure using laser engineered net shaping. Mater. Lett. **216**, 16-19 (2018).
DOI: https://doi.org/10.1016/j.matlet.2017.12.129

[34] B. Chen, Y. Su, Z. Xie, C. Tan, J. Feng, Development and characterization of 316L/Inconel 625 functionally graded material fabricated by laser direct metal deposition. Opt. Laser Technol. **123**, 105916 (2020).
DOI: https://doi.org/10.1016/j.optlastec.2019.105916

[35] N. Chen, H.A. Khan, Z. Wan, J. Lippert, H. Sun, S.L. Shang, Microstructural characteristics and crack formation in additively manufactured bimetal material of 316L stainless steel and Inconel 625. Addit. Manuf. **32**, 101037 (2020).
DOI: https://doi.org/10.1016/j.addma.2020.101037

[36] O. Mehrabi, S.M.H. Seyedkashi, M. Moradi, Functionally graded additive manufacturing of thin-walled 316L stainless steel–Inconel 625 by direct laser metal deposition process: characterization and evaluation. Metals **13** (6), 1-18 (2023).
DOI: https://doi.org/10.3390/met13061108

[37] U. Savitha, G. Jagan Reddy, A. Venkataramana, A. Sambasiva Rao, A.A. Gokhale, M. Sundararaman, Chemical analysis, structure and mechanical properties of discrete and compositionally graded SS316–IN625 dual materials. Mater. Sci. Eng. A **647**, 344-352 (2015). DOI: https://doi.org/10.1016/j.msea.2015.09.001

[38] R. Koike, I. Unotoro, Y. Akinuma, T. Aoyama, Y. Oda, Evaluation for mechanical characteristics of Inconel 625–SUS316L joint produced with direct energy deposition. Procedia Manuf. **14**, 105-110 (2017).
DOI: https://doi.org/10.1016/j.promfg.2017.11.012

[39] X. Zhang, Y. Chen, F. Liou, Fabrication of SS316L–IN625 functionally graded materials by powder-fed directed energy deposition. Sci. Technol. Weld. Join. **24** (5), 1-13 (2019).
DOI: https://doi.org/10.1080/13621718.2019.1589086

[40] X. Li, P. Jiang, M. Nie, Z. Liu, M. Liu, Y. Qiu et al., Enhanced strength–ductility synergy of laser additive manufactured stainless steel/Ni-based superalloy dissimilar materials characterized by bionic mechanical interlocking structures. J. Mater. Res. Technol. **26**, 4770-4783 (2023).
DOI: https://doi.org/10.1016/j.jmrt.2023.08.217

[41] S.C. Bodner, K. Hlushko, L.T.G. Van de Vorst, J. Meindlhumer Todt, M.A. Nielsen, Graded Inconel–stainless steel multi-material structure by inter- and intralayer variation of metal alloys. J. Mater. Res. Technol. **21**, 4846-4859 (2022).
DOI: https://doi.org/10.1016/j.jmrt.2022.11.064

[42] B.E. MacDonald, B. Zheng, B. Fields, X. Wang, S. Jiang, P. Cao, Influence of co-deposition strategy on the mechanical behavior of additively manufactured functionally integrated materials. Addit. Manuf. **61**, 103328 (2023).
DOI: https://doi.org/10.1016/j.addma.2022.103328

[43] I. Noh, J. Jeon, S.W. Lee, A study on metallographic and machining characteristics of functionally graded material produced by directed energy deposition. Crystals **13** (10), 1-17 (2023).
DOI: https://doi.org/10.3390/cryst13101491

[44] N. Sargent, Y. Wang, D. Li, Y. Zhao, X. Wang, W. Xiong, Exploring alloy design pathway through directed energy deposition of powder mixtures: a study of stainless steel 316L and Inconel 718. Addit. Manuf. Lett. **6**, 100133 (2023).
DOI: https://doi.org/10.1016/j.addlet.2023.100133

[45] N. Sommer, A. Bauer, M. Kahlmeyer, T. Wegener, S. Degener, A. Liehr, High-throughput alloy development using advanced characterization techniques during directed energy deposition additive manufacturing. Adv. Eng. Mater. **25** (15), 1-11 (2023).
DOI: https://doi.org/10.1002/adem.202300030

[46] J.F.S. Markanday, Applications of alloy design to cracking resistance of additively manufactured Ni-based alloys. Mater. Sci. Technol. **38** (16), 1300-1314 (2022).
DOI: https://doi.org/10.1080/02670836.2022.2068759

[47] H. Kahya, H. Gurun, G. Kucukturk, Experimental and analytical investigation of the re-melting effect in the manufacturing of 316L by direct energy deposition (DED) method. Metals **13** (6), 1-19 (2023). DOI: https://doi.org/10.3390/met13061144

[48] A. Saboori, A. Aversa, G. Marchese, S. Biamino, M. Lombardi, P. Fino, Microstructure and mechanical properties of AISI 316L produced by directed energy deposition-based additive manufacturing: a review. Appl. Sci. **10** (9), 1-23 (2020).
DOI: https://doi.org/10.3390/app10093310

[49] S. Samuha, J. Bickel, T. Mukherjee, T. DebRoy, T.J. Lienert, S.A. Maloy et al., Mechanical performance and microstructure of the grade 91 stainless steel produced via directed energy deposition laser technique. Mater. Des. **227**, 111804 (2023).
DOI: https://doi.org/10.1016/j.matdes.2023.111804

[50] H. Khodashenas, H. Mirzadeh, Post-processing of additively manufactured high-entropy alloys – A review. J. Mater. Res. Technol. **21**, 3795-3814 (2022).
DOI: https://doi.org/10.1016/j.jmrt.2022.11.027

[51] M. Dadkhah, J.M. Tulliani, A. Saboori, L. Iuliano, Additive manufacturing of ceramics: advances, challenges, and outlook. J. Eur. Ceram. Soc. **43** (15), 6635-6664 (2023).
DOI: https://doi.org/10.1016/j.jeurceramsoc.2023.07.033

[52] G. Piscopo, E. Atzeni, A. Saboori, A. Salmi, An overview of physical phenomena involved in the laser powder directed energy deposition process. Preprints 2022, 1-34 (2022).
DOI: https://doi.org/10.20944/preprints202211.0397.v1

[53] A. Singh, S. Kapil, M. Das, A comprehensive review of the methods and mechanisms for powder feedstock handling in directed energy deposition. Addit. Manuf. **35**, 101388 (2020).
DOI: https://doi.org/10.1016/j.addma.2020.101388

[54] A. Guner, P. Bidare, A. Jiménez, S. Dimov, K. Essa, Nozzle designs in powder-based direct laser deposition: a review. Int. J. Precis. Eng. Manuf. **23** (9), 1077-1094 (2022).
DOI: https://doi.org/10.1007/s12541-022-00688-1

[55] B. Dikra, F. Mamoun, M. Abla, B. Régis, O. Aleksei, R. Mohammed, High photocatalytic capacity of porous ceramic-based powder doped with MgO. J. Korean Ceram. Soc. **60**, 155-168 (2023). DOI: https://doi.org/10.1007/s43207-022-00254-5

[56] W. Meng, Z. Wenhao, Z. Wang, X. Yin, B. Cui, Fabrication of steel–Inconel functionally graded materials by laser melting deposition integrating with laser synchronous preheating. Opt. Laser Technol. **131**, 106451 (2020).
DOI: https://doi.org/10.1016/j.optlastec.2020.106451